Detection of over-ground petroleum and gas pipelines from optical remote sensing images

Detection of over-ground petroleum and gas pipelines from optical remote sensing images

Huan Chang[a], Lu Bai[b], Zhibao Wang[a,c], Mei Wang[a], Ying Zhang[d,e], Jinhua Tao[d,e], Liangfu Chen[d,e]
[a]School of Computer and Information Technology, Northeast Petroleum University, Daqing, China
[b]School of Electronics, Electrical Engineering and Computer Science, Queen's University Belfast, Belfast, UK
[c]Bohai-Rim Energy Research Institute, Northeast Petroleum University, Qinhuangdao, China
[d]State Key Laboratory of Remote Sensing Science, Aerospace Information Research Institute, Chinese Academy of Sciences, Beijing, China
[e]University of Chinese Academy of Sciences, Beijing, China

ABSTRACT

Petroleum and gas pipelines, comprising petroleum and gas pipes and related components, play an irreplaceable role in petroleum and gas transportation. For global economic growth, petroleum and gas are crucial natural resources. However, the pipelines often cross permafrost regions with challenging working conditions. Additionally, the potential for natural disasters raises concerns about pipeline accidents, posing a threat to pipeline operational safety. In response to the complexity of pipeline supervision and management, we choose to use remote sensing method combining deep learning-based algorithms. In this work, we build a petroleum and gas pipes dataset, which includes 1,388 remote sensing images and the study area is Russian polar regions. We trained FCN and U-Net deep learning models by using our self-built dataset for the detection of petroleum and gas pipes. Models' performances were evaluated using MIoU (Mean Intersection over Union), mean precision, mean recall to evaluate the accuracy of the model's prediction results and compared them visually with ground truth. Our results find that deep learning models can effectively learn the characteristics of pipelines and achieve ideal detection results on our dataset. The MIoU of the FCN model achieved 0.885 and the U-Net model achieved 0.894. The results demonstrate that our trained models can be used to accurately identify the petroleum and gas pipelines in remote sensing images.

Keywords: Semantic Segmentation, U-Net, FCN, petroleum and gas pipes

1. INTRODUCTION

Pipelines have emerged as a trusted means to transfer oil and gas products across wide distances due to their inherent safety and suitability[1]. Petroleum and gas pipelines are composed of petroleum and gas pipes, their corresponding accessories and integrated pump units tailored to the process flow requirement. They are designed and installed into a complete pipeline system, facilitating essential tasks such as petroleum and gas loading, unloading and transportation. As global petroleum and gas fields continuously grow in various regions across the world, the construction of petroleum and gas pipelines has experienced rapid expansion, fueled by the escalating demand for global economic progress. However, many natural hazards such as earthquake, floods and lightning can cause accidents of pipelines and have threaten the operational safety of the pipelines[2,3]. The pipelines often traverse vast areas of permafrost areas, which are characterised by strong winds and obvious annual temperature fluctuations. The climate conditions in the pipeline laying area are harsh, making it difficult for humans to detect and repair pipeline faults in a timely manner. In addition, there is lack of documentation of installed petroleum and gas pipes and current studies of petroleum and gas pipelines are mainly carried out through on-site investigation[4].

Remote sensing provides numerous benefits in oil and pipeline detection. It offers wide coverage, timely data acquisition, and non-intrusive monitoring, especially in challenging environments. The recent development of remote sensing techniques and machine learning based algorithms of image processing has enabled the remote detection of over-ground petroleum and gas pipelines from remote sensing images. Machine learning methods in particular deep learning based methods have shown good performance on drainage pipes detection from remote sensing images[5–7]. Deep learning methods aid stakeholders to recognise the earliest phases of threats to the pipelines, supplying them timely insights for effective problem resolution[7]. Therefore, in this work we explored the feasibility of detecting over-ground petroleum and gas pipelines from remote sensing images using deep learning-based algorithms.

2. RELATED WORK

With the development of remote sensing satellite technology, the remote sensing images have greatly improved in resolution, recognition, timeliness, and effectiveness[8–11], which makes it possible to the automatic detection of different ground objects from satellite or aerial remote sensing images[12], including vehicles[13], buildings[14], vegetation[15], water bodies[16], infrastructure[17], and urban features[18]. Extensive research has been undertaken in the realm of detecting infrastructures associated with oil and gas operations. The detection of oil tanks has been a thoroughly explored domain, and various approaches have been employed, ranging from traditional image processing techniques to cutting-edge deep learning algorithms[19–21]. Additionally, the detection of oil spills has attracted significant attention within the realm of environmental monitoring and disaster management[22]. More recently, there has been a notable surge in research efforts focused on the detection of objects associated with oil fields[23]. This emerging area of study aims to identify and analyse various elements within oil field environments, ranging from infrastructure and equipment to natural features. Wang et al.[24] have established an oil well dataset and conducted a comprehensive evaluation of the state of the art deep learning models utilising advanced object detection algorithms on this dataset. He et al.[25] has introduced an innovative instance segmentation approach based on Convolutional Neural Networks (CNNs) for the identification and extraction of oil well sites. With the rapid development of deep learning technology, the role of deep convolutional neural networks in object detection is becoming more and more important. Compared with traditional methods which mainly rely on manual features, object detection methods based on deep learning can automatically learn low-level and high-level features of an image. Image features learned by deep learning technology are more representative than manually extracted features[26].

The rapid acquisition of remote sensing information is of great research significance for the development of image semantic segmentation methods in remote sensing image interpretation applications. With the increasing variety of data recorded in satellite remote sensing images and the increasing complexity of feature information, accurately and effectively extracting information from remote sensing images has become the key to interpreting remote sensing images using image semantic segmentation methods. In order to explore fast and efficient image semantic segmentation methods for interpreting remote sensing images, a large number of image semantic segmentation methods have emerged for remote sensing images[27].Li et al[28] has proposed a novel approach involving semantic segmentation of remote sensing images through self-supervised multitask representation learning. This method aims to capture impactful visual representations for enhanced interpretation of remote sensing imagery. Liu et al. [29] introduced an innovative semantic segmentation framework named Positioning Guidance Network (PGNet) for Very High-Resolution (VHR) remote sensing images. This framework comprises three essential components: a feature extractor, a positioning guiding module (PGM), and a self-multiscale collection module (SMCM).

3. DATASET

In this study, we have built a dataset for the over-ground petroleum and gas pipelines using remote sensing images obtained from the WayBack Imagery[30]. Wayback Imagery is a digital archive of the World Imagery base map, enabling users to access different versions of World Imagery captured over years. Our dataset is constructed using WayBack images from June 8, 2022, encompassing the Arctic region of Russia, with the total petroleum and gas pipeline length approximating 917 km. Our dataset contains a total of 1388 remote sensing images. Each image within the dataset spans 400m in length and 400m in width, covering a total area of 1.6km². The resolution of each image within our dataset is 512×512 pixels. Petroleum and gas pipelines were annotated by researchers with experience in remote sensing images annotation. A geographic information processing software – ArcGIS was used in the annotation task. Example images from our dataset are shown in Figure 1 below.

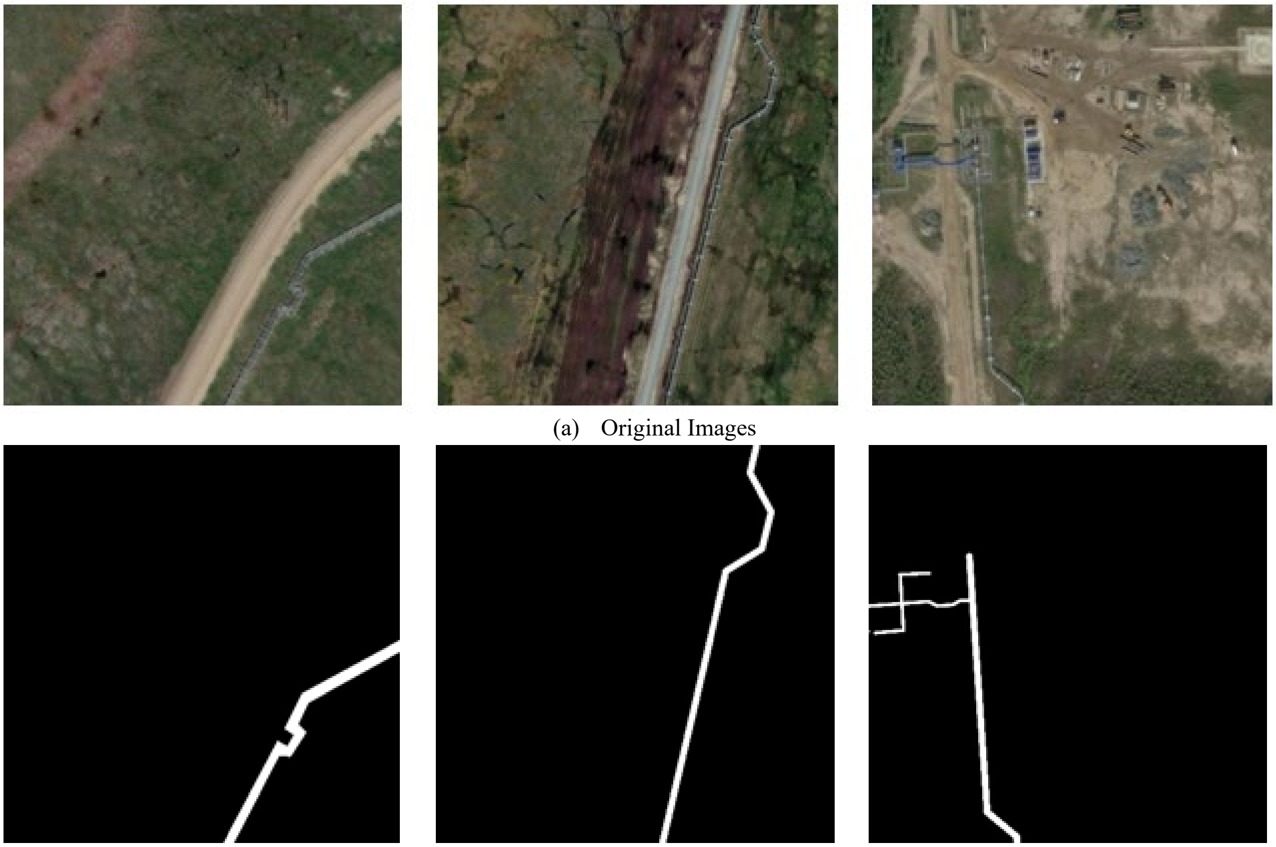
(a) Original Images

(b) Annotated labels

Figure 1. Examples of the Original images and their annotated labels from our built dataset.

4. METHODOLOGY

It is widely known that remote sensing images exhibit intricate spectral, shape and texture characteristics. Distinct objects from the remote sensing images have their unique attributes. Deep learning neural networks can be used to extract these intricate features from remote sensing images. Inspired by the work done on underground drainage pipes with linear characteristics from remote sensing images by Breitkopf et al.[6], FCN and U-Net models were used in this work to extract the characteristics of the over-ground petroleum and gas pipelines from remote sensing images. FCN has been widely used in remote sensing semantic segmentation. U-Net has improved based on FCN. U-Net architecture[31] is a fully convolutional auto-encoder network, which contains a contracting and an expanding path. The contracting path captures context, whereas the expanding path allows precise localisation. These two pathways maintain a symmetric configuration. The U-Net can make use of skip connections that make it possible for the model to be trained with fewer images when working with a limited dataset.

As shown in Figure 2, the U-Net network comprises an encoder (on the left) and a decoder (on the right). In this study, we have adopted a five-layer network structure. Throughout the architecture, all convolution operations employ a 3×3 convolution kernel, with a stride and padding value of 1. The chosen activation function is Rectified Linear Unit (ReLU)[32]. Within the encoder, depth is increased by a convolution operation and coupled with the application of a 2x2 max polling operation with a stride of 2. Meanwhile, the decoder employs 2x2 upsampling to magnify the feature map's dimension.

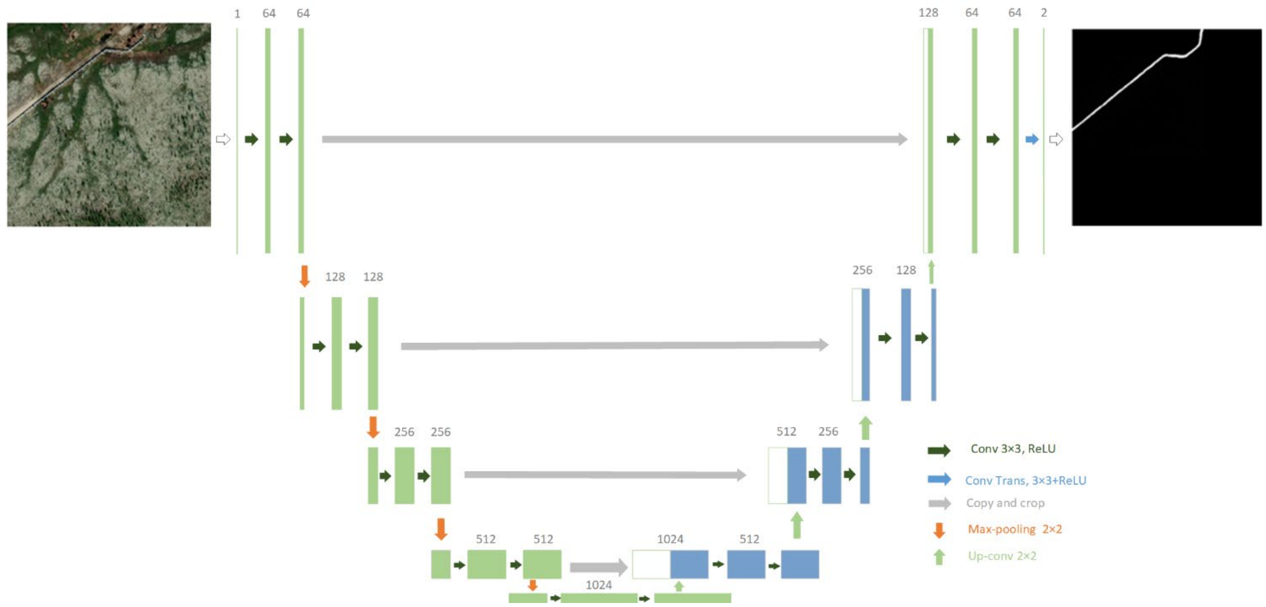

Figure. 2 Structure diagram of remote sensing image semantic segmentation model based on U-Net

5. EXPERIMENT AND RESULTS

5.1 Experiment details

Experiments were conducted on our self-built dataset. We used 1200 images of the training set to train the two models – FCN and U-Net respectively and evaluate the models using the remaining 188 images of the test set. The experimental environment of this work is based on an Ubuntu operating system. Python is used as the main programming language and PyTorch library is used for deep learning model implementation. The training time of FCN and U-Net model is 6 hours and 5 hours respectively, and the test time is 4 minutes and 2 minutes, respectively.

5.2 Model evaluation metrics

To evaluate the performance of the proposed model, we choose to use three evaluation metrics including MIoU (Mean Intersection over Union), mean precision and mean recall. Based on the mentioned above, MIoU, mean precision, and mean recall are calculated by using equations (1)(2)(3) respectively. Among them, k is the total number of categories, P_k is the predicted value for the k-th category, G_k is the true value of the k-th category.

MIoU quantifies the overlap between predicted and actual values within each category, by dividing the intersection by the union and subsequently calculating the average. It reflects the segmentation performance for individual categories, with a higher value indicating better performance. The formula for calculating MIoU is as follows:

$$MIoU = \frac{1}{k}\sum_{k=1}^{k}\frac{P_k \cup G_k}{P_k \cap G_k} \tag{1}$$

Mean precision is computed by dividing the count of accurate predictions within each category by the overall number of predictions for that specific category, followed by calculating the average across categories. It reflects the model's ability to distinguish between different categories, with higher score indicating a stronger discriminative capability. The formula for calculating mean precision is as follows:

$$mean\ precision = \frac{1}{k}\sum_{k=1}^{k}\frac{P_k \cup G_k}{P_k} \tag{2}$$

Mean recall is determined by dividing the count of accurately predicted items within each category by the total number of items present in that specific category. Subsequently, an average is calculated across all categories. It reflects the model's effectiveness in covering instances of each category, with a higher value indicating better coverage capabilities. The formula for calculating mean recall is as follows:

$$mean\ recall = \frac{1}{k}\sum_{k=1}^{k}\frac{P_k \cup G_k}{G_k} \tag{3}$$

5.3 Experimental results

The detection results of the two distinct models are as shown in Figure 3. First column of Figure 3 shows the original petroleum and gas pipelines in remote sensing images. Second and third columns of Figure 3 are the detection outputs from the FCN model and U-Net model respectively. In these representations, the white part refers to the detected petroleum and gas pipelines, and the black part refers to the background.

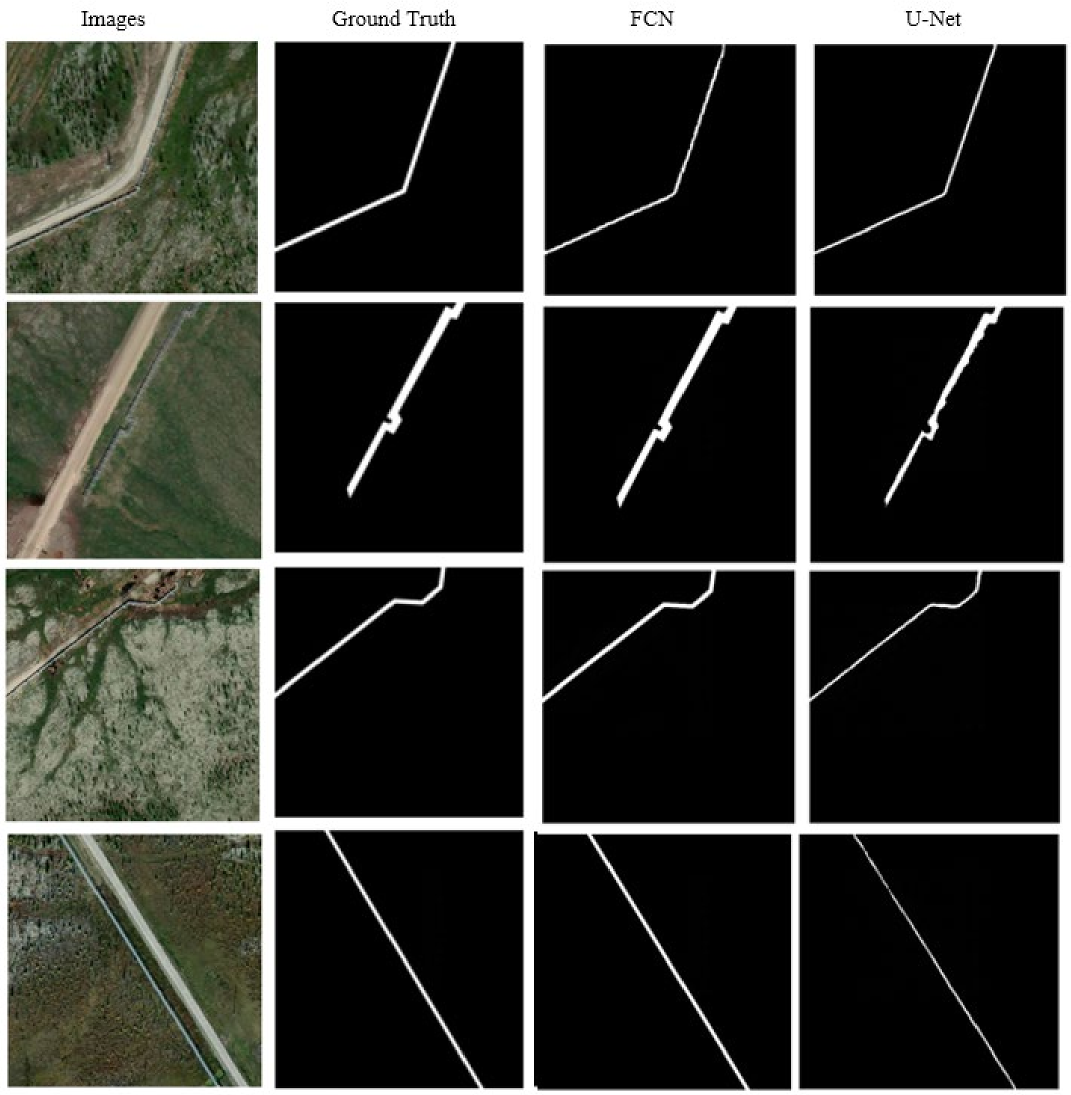

Figure 3. Experimental Results of the FCN and U-Net models. Images column indicates the actual image within the dataset, and Label column indicates the actual annotated label. The third column represents the outcomes of FCN model, and the fourth column represents the outcomes of U-Net model.

To evaluate the model performances, mean precision, mean recall and MIoU were used. The MIoU of U-Net model achieved at 0.894 is better than the MIoU of FCN model which is 0.885. Table 1 presents the MIoU, mean precision, and mean recall values for the test set within our dataset. The results indicate that the model trained using deep learning has the capability to identify petroleum and gas pipelines in satellite images.

Table 1. MIoU, mean precision and mean recall of the test set of our dataset.

Model	MIoU	Mean Precision	Mean Recall
FCN	0.885	0.939	0.929
U-Net	**0.894**	**0.940**	**0.936**

6. CONCLUSIONS

In this work, we use satellite imagery sourced from WayBack Image to construct a remote sensing dataset focusing on petroleum and gas pipeline. The experimental results show that FCN and U-Net networks have the ability to learn the characteristics of pipelines and can accurately identify the pipelines by through models trained on a large number of satellite imagery related to pipelines. In future, we plan to expand our dataset by including petroleum and gas pipelines of different regions across the world and include more samples with complex background. Also, in order to further detection accuracy, we intend to explore more models to train our dataset and incorporate active learning strategies to improve sample selection methods.

REFERENCES

[1] Khan, F. I. and Amyotte, P. R., "Inherent safety in offshore oil and gas activities: a review of the present status and future directions," Journal of Loss Prevention in the Process Industries **15**(4), 279–289 (2002).

[2] Girgin, S. and Krausmann, E., "Historical analysis of U.S. onshore hazardous liquid pipeline accidents triggered by natural hazards," Journal of Loss Prevention in the Process Industries **40**, 578–590 (2016).

[3] Petrova, E. G., "Natural factors of technological accidents: the case of Russia," Nat. Hazards Earth Syst. Sci. **11**(8), 2227–2234 (2011).

[4] Yan, Y., Ma, S., Yin, S., Hu, S., Long, Y., Xie, C. and Jiang, H., "Detection and numerical simulation of potential hazard in oil pipeline areas based on UAV surveys," Frontiers in Earth Science **9**, 665478 (2021).

[5] Cho, E., Jacobs, J. M., Jia, X. and Kraatz, S., "Identifying Subsurface Drainage using Satellite Big Data and Machine Learning via Google Earth Engine," Water Resources Research **55**(10), 8028–8045 (2019).

[6] Breitkopf, T. L., Hackel, L., Ravanbakhsh, M., Cooke, A.-K., Willkommen, S., Broda, S. and Demir, B., "Advanced deep learning architectures for accurate detection of subsurface tile drainage pipes from remote sensing images," Image and Signal Processing for Remote Sensing XXVIII **12267**, 181–188, SPIE (2022).

[7] Woo, D. K., Ji, J. and Song, H., "Subsurface drainage pipe detection using an ensemble learning approach and aerial images," Agricultural Water Management **287**, 108455 (2023).

[8] Liu, Y., Zuo, X., Tian, J., Li, S., Cai, K. and Zhang, W., "Research on Generic Optical Remote Sensing Products: A Review of Scientific Exploration, Technology Research, and Engineering Application," IEEE J. Sel. Top. Appl. Earth Observations Remote Sensing **14**, 3937–3953 (2021).

[9] Wang, Z., Zhang, Z., Bai, L., Yang, Y. and Ma, Q., "Application of an Improved U-Net Neural Network on Fracture Segmentation from Outcrop Images," IGARSS 2022 - 2022 IEEE International Geoscience and Remote Sensing Symposium, 3512–3515, IEEE, Kuala Lumpur, Malaysia (2022).

[10] Shi, K., Bai, L., Wang, Z., Tong, X., Mulvenna, M. D. and Bond, R. R., "Photovoltaic Installations Change Detection from Remote Sensing Images Using Deep Learning," IGARSS 2022 - 2022 IEEE International Geoscience and Remote Sensing Symposium, 3231–3234, IEEE, Kuala Lumpur, Malaysia (2022).

[11] Zhang, J., Wang, Z., Bai, L., Song, G., Tao, J. and Chen, L., "Deforestation Detection Based on U-Net and LSTM in Optical Satellite Remote Sensing Images," 2021 IEEE International Geoscience and Remote Sensing Symposium IGARSS, 3753–3756, IEEE, Brussels, Belgium (2021).

[12] Cheng, G. and Han, J., "A survey on object detection in optical remote sensing images," ISPRS Journal of Photogrammetry and Remote Sensing **117**, 11–28 (2016).

[13] Ji, H., Gao, Z., Mei, T. and Ramesh, B., “Vehicle Detection in Remote Sensing Images Leveraging on Simultaneous Super-Resolution,” IEEE Geosci. Remote Sensing Lett. **17**(4), 676–680 (2020).
[14] Li, J., Huang, X., Tu, L., Zhang, T. and Wang, L., “A review of building detection from very high resolution optical remote sensing images,” GIScience & Remote Sensing **59**(1), 1199–1225 (2022).
[15] Kattenborn, T., Leitloff, J., Schiefer, F. and Hinz, S., “Review on Convolutional Neural Networks (CNN) in vegetation remote sensing,” ISPRS Journal of Photogrammetry and Remote Sensing **173**, 24–49 (2021).
[16] Bijeesh, T. V. and Narasimhamurthy, K. N., “Surface water detection and delineation using remote sensing images: a review of methods and algorithms,” Sustain. Water Resour. Manag. **6**(4), 68 (2020).
[17] Schnebele, E., Tanyu, B. F., Cervone, G. and Waters, N., “Review of remote sensing methodologies for pavement management and assessment,” Eur. Transp. Res. Rev. **7**(2), 7 (2015).
[18] Li, W., Liu, H., Wang, Y., Li, Z., Jia, Y. and Gui, G., “Deep Learning-Based Classification Methods for Remote Sensing Images in Urban Built-Up Areas,” IEEE Access **7**, 36274–36284 (2019).
[19] Ok, A. O. and Baseski, E., “Circular Oil Tank Detection From Panchromatic Satellite Images: A New Automated Approach,” IEEE Geosci. Remote Sensing Lett. **12**(6), 1347–1351 (2015).
[20] Liu, Z., Zhao, D., Shi, Z. and Jiang, Z., “Unsupervised Saliency Model with Color Markov Chain for Oil Tank Detection,” Remote Sensing **11**(9), 1089 (2019).
[21] Zhu, M., Wang, Z., Bai, L., Zhang, J., Tao, J. and Chen, L., “Detection of industrial storage tanks at the city-level from optical satellite remote sensing images,” Image and Signal Processing for Remote Sensing XXVII, L. Bruzzone, F. Bovolo, and J. A. Benediktsson, Eds., 33, SPIE, Online Only, Spain (2021).
[22] Seydi, S. T., Hasanlou, M., Amani, M. and Huang, W., “Oil Spill Detection Based on Multiscale Multidimensional Residual CNN for Optical Remote Sensing Imagery,” IEEE J. Sel. Top. Appl. Earth Observations Remote Sensing **14**, 10941–10952 (2021).
[23] Song, G., Wang, Z., Bai, L., Zhang, J. and Chen, L., “Detection of oil wells based on faster R-CNN in optical satellite remote sensing images,” Image and Signal Processing for Remote Sensing XXVI, C. Notarnicola, F. Bovenga, L. Bruzzone, F. Bovolo, J. A. Benediktsson, E. Santi, and N. Pierdicca, Eds., 17, SPIE, Online Only, United Kingdom (2020).
[24] Wang, Z., Bai, L., Song, G., Zhang, J., Tao, J., Mulvenna, M. D., Bond, R. R. and Chen, L., “An Oil Well Dataset Derived from Satellite-Based Remote Sensing,” Remote Sensing **13**(6), 1132 (2021).
[25] He, H., Xu, H., Zhang, Y., Gao, K., Li, H., Ma, L. and Li, J., “Mask R-CNN based automated identification and extraction of oil well sites,” International Journal of Applied Earth Observation and Geoinformation **112**, 102875 (2022).
[26] Zhao, Z.-Q., Zheng, P., Xu, S.-T. and Wu, X., “Object Detection With Deep Learning: A Review,” IEEE Trans. Neural Netw. Learning Syst. **30**(11), 3212–3232 (2019).
[27] Yuan, X., Shi, J. and Gu, L., “A review of deep learning methods for semantic segmentation of remote sensing imagery,” Expert Systems with Applications **169**, 114417 (2021).
[28] Li, W., Chen, H. and Shi, Z., “Semantic Segmentation of Remote Sensing Images With Self-Supervised Multitask Representation Learning,” IEEE J. Sel. Top. Appl. Earth Observations Remote Sensing **14**, 6438–6450 (2021).
[29] Liu, B., Hu, J., Bi, X., Li, W. and Gao, X., “PGNet: Positioning Guidance Network for Semantic Segmentation of Very-High-Resolution Remote Sensing Images,” Remote Sensing **14**(17), 4219 (2022).
[30] “Wayback Imagery.”, <https://www.arcgis.com/home/group.html?id=0f3189e1d1414edfad860b697b7d8311#overview>.
[31] Ronneberger, O., Fischer, P. and Brox, T., “U-net: Convolutional networks for biomedical image segmentation,” Lecture Notes in Computer Science (including subseries Lecture Notes in Artificial Intelligence and Lecture Notes in Bioinformatics) (2015).
[32] Agarap, A. F., “Deep learning using rectified linear units (relu),” arXiv preprint arXiv:1803.08375 (2018).